Multiphoton fusion of light nuclei in intense laser fields

Binbing Wu,[1] Zhengfeng Fan,[1,3,*] Difa Ye,[1] Tao Ye,[1] Congzhang Gao,[1] Chengxin Yu,[1] Xuefeng Xu,[1] Cunbo Zhang,[1] and Jie Liu[2,3,†]

[1]*Institute of Applied Physics and Computational Mathematics, Beijing 100088, People's Republic of China*
[2]*Graduate School, China Academy of Engineering Physics, Beijing 100193, People's Republic of China*
[3]*CAPT, HEDPS, and IFSA Collaborative Innovation Center of MoE, Peking University, Beijing 100871, People's Republic of China*

(Received 1 January 2024; revised 21 March 2024; accepted 30 May 2024; published 17 June 2024)

We investigate the fusion cross sections of light nuclei in the presence of linearly polarized intense laser fields. By combining the Coulomb-Volkov solutions with the complex spherical square-well nuclear potential, we derive an explicit formulation of the multiphoton cross section in a self-consistent manner. Our analysis is specifically focused on deuteron-triton (DT) and proton-boron (p ^{11}B) fusion reactions, both of which have garnered widespread attention. The theoretical results reveal that, under conditions of longer laser wavelengths and lower incident particle kinetic energies, a few thousands of photons can participate in the fusion reactions, resulting in a substantial enhancement of fusion cross sections by almost ten orders of magnitude. We elucidate the multiphoton mechanism underlying these findings and discuss their implications.

DOI: 10.1103/PhysRevC.109.064615

I. INTRODUCTION

The investigation of light-matter interactions holds a prominent position in physics research [1,2]. The identification of multiphoton ionization [3,4] in atoms and molecules exposed to intense laser fields has unveiled the nonperturbative regime in strong laser fields [1]. This discovery has paved the way for diverse nonperturbative phenomena, including higher-order above-threshold ionization [5], nonsequential double ionization [6], and high-order harmonic generation [7,8].

In recent years, advancements in the chirped-pulse amplification (CPA) technique have increased laser intensity to 10^{23} W/cm^2 [9]. Furthermore, the Extreme Light Infrastructure for Nuclear Physics (ELI-NP) in Europe is poised to generate high-intensity lasers at 10^{25} W/cm^2 in the near future [10]. These strong laser fields impact not only atomic and molecular processes [1,2] but also nuclear processes [11–32]. For instance, recent theoretical studies reveal that intense laser fields can excite ^{229}Th to isomeric states through electron recollision [12,13], and can influence the half-life of α decay from heavy nuclei by modifying the Coulomb barrier [14–17], etc. However, some other analyses seem to show that present-day lasers cannot influence the half-life of α decay measurably [33–40].

The exploration of fusion cross section for light nuclei under intense laser fields has attracted extensive attention owing to its potential application in clean energy sources [18–32]. Previous studies [18–24,26–28,30,31] mainly utilize the celebrated Gamow form [41,42] for fusion cross section and focus on the enhancement effects on tunneling probability through the Coulomb repulsive potential. However, these approaches lack a self-consistent description of the nuclear potential combined with the Coulomb repulsion potential in intense laser fields. Given the intricate nature of the nuclear potential, the phenomenological optical potentials within the mean-field approximation find extensive use in describing the nuclear potential [43–47]. A complex spherical square-well optical potential is commonly employed to characterize nuclear potentials in the context of light nuclear fusion [44–47], wherein the imaginary component of the potential signifies the decay of the compound nucleus. In our recent work [25], applying a complex spherical square-well model and exploiting Kramers's approximation, we observed the distinct shift in the peaks of fusion cross section within strong high-frequency laser fields, attributed to resonant tunneling mechanism. Intense low-frequency laser fields, particular in the near-infrared regime, are generated by a majority of advanced laser facilities worldwide [48]. In scenarios of intense low-frequency fields, a substantial number of photons (e.g., $>10\,000$) are involved. These laser photons are extensively employed to investigate the multiphoton ionization of atomic and molecular systems [1,2]. The question of whether multiphoton processes can affect the light nuclear cross section remain unresolved.

In this study, we extend our recent theoretical work [25] to the low-frequency regime, where a complex spherical square well [44–47] is employed to characterize the nuclear potential. Utilizing the Coulomb-Volkov solutions which are successfully employed in handing nonperturbative multiphoton process in the electron-atom collision [49], we self-consistently derive the multiphoton cross sections of nuclear fusion. Our specific focus is on deuteron-triton (DT) and proton-boron (p ^{11}B) fusion. (Here and in the following "D" and "T" denote "^{2}H" and "^{3}H", respectively.) DT

*Contact author: fan_zhengfeng@iapcm.ac.cn
†Contact author: jliu@gscaep.ac.cn

fusion takes precedence in controlled fusion research owing to its relatively high fusion cross section compared to other fusion reactions [42]. On the other hand, p ^{11}B fusion reaction is an aneutronic process involving abundant and stable isotopes [50–52]. The potential applications of this reaction span from controlled nuclear fusion to an emerging form of proton-boron capture therapy [51,52]. Our findings reveal that for longer laser wavelengths and lower incident particle kinetic energies, fusion cross sections exhibit substantial enhancement for both DT and p ^{11}B fusion reactions due to multiphoton processes.

The structure of this work is outlined as follows: Section II introduces our theoretical framework for multiphoton fusion. Section III presents our main results and discussions. Section IV provides the main conclusions and outlooks.

II. THEORETICAL FRAMEWORK

In this section, we present a theoretical model for examining multiphoton fusion in the presence of a background laser field. The laser field is assumed to be a monochromatic wave with frequency ω and linear polarized along the z axis. Under the dipole approximation, it is described by the uniform and time varying vector potential $\boldsymbol{A}(t) = A_0 \cos(\omega t)\vec{e}_z$, where A_0 is the amplitude.

In the presence of laser fields, the relative motion of a two-body, spinless fusion system in the center-of-mass (CM) frame can be described by the time-dependent Schrödinger equation

$$i\hbar\frac{\partial}{\partial t}\Psi(t,\boldsymbol{r}) = \left[\frac{1}{2\mu}(\hat{\boldsymbol{P}} - q_{\rm eff}\boldsymbol{A}(t))^2 + V(r)\right]\Psi(t,\boldsymbol{r}), \quad (1)$$

where $\mu = m_{\rm p}m_{\rm t}/(m_{\rm p}+m_{\rm t})$ is the reduced mass of two nuclei. $m_{\rm p}$ and $m_{\rm t}$ are masses of incident projectile and target nuclei, respectively. $q_{\rm eff} = e(Z_{\rm p}m_{\rm t} - Z_{\rm t}m_{\rm p})/(m_{\rm p}+m_{\rm t})$ is an effective charge, where $Z_{\rm p}$ and $Z_{\rm t}$ are charge numbers of incident projectile and target nuclei, respectively. As illustrated in Fig. 1, the potential $V(r)$ of the fusion process is characterized by a short-range complex square nuclear potential with a long-range Coulomb repulsive potential between two nuclei. The expression for $V(r)$ is given by

$$V(r) = \begin{cases} V_{\rm r} + iV_{\rm i}, & r < r_{\rm N}, \\ \frac{e^2}{4\pi\epsilon_0 r}, & r > r_{\rm N}, \end{cases} \quad (2)$$

where $r_{\rm N}$ is the radius of nuclear well, i is the unit imaginary number, and ϵ_0 is vacuum permittivity. $V_{\rm r}$ and $V_{\rm i}$ can describe the scattering and absorption effects during the fusion, respectively, which be known as the "optical model." Comparing with experimental benchmark cross section data in the absence of electromagnetic fields, the three optical parameters $V_{\rm r}$, $V_{\rm i}$, and $r_{\rm N}$ for light fusion reactions were calibrated in our recent work [47].

A. Solution by expansion on spherical Coulomb-Volkov states

We attempt to solve the time-dependent Schrödinger equation (1) by the expansion on spherical Coulomb-Volkov states. According to the quantum scattering theory, the wave function $\Psi(t,\boldsymbol{r})$ after being scattered by the ansatz can be written as the sum of an incoming wave $\Psi_{\rm inc}$ and a scattered wave $\Psi_{\rm scatt}$:

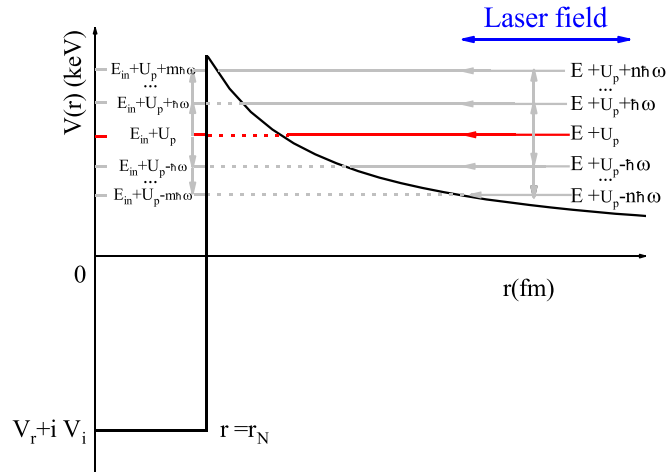

FIG. 1. A schematic representation of the model for multiphoton fusion processes in the presence of a linearly polarized laser field. The potential $V(r)$ is considered to be a short-range complex spherical square well with a long-range Coulomb repulsive potential between two nuclei. The charge particle within a intense laser field exhibits a range of possible energies due to multiphoton processes. Here, E represents the kinetic energy of fusion system in the CM frame, U_p denotes the ponderomotive energy of the particle in the laser fields, and n corresponds the number of photons absorbed or emitted outside nuclear potential. $E_{\rm in}$ is the energy within the nuclear potential, and m represents the number of photons absorbed or emitted inside the nuclear potential.

$$\begin{aligned}\Psi(t,\boldsymbol{r}) &= \Psi_{\rm inc}(t,\boldsymbol{r}) + \Psi_{\rm scatt}(t,\boldsymbol{r}) \\ &= \sum_{l=0}^{+\infty}(2l+1)i^l\frac{F_l(k_n r,\eta_n)}{k_n r}P_l(\vartheta)e^{-\frac{i}{\hbar}Et}e^{-\frac{i}{\hbar}\int_{-\infty}^{t}V_L d\tau} \\ &\quad + \sum_{n=-\infty}^{+\infty}\sum_{l=0}^{+\infty}(2l+1)i^l A_{n,l}\frac{H_l(k_n r,\eta_n)}{k_n r} \\ &\quad \times P_l(\vartheta)e^{-\frac{i}{\hbar}E_n t}, \quad r > r_N, \end{aligned} \quad (3)$$

where F_l is regular Coulomb wave function [53], P_l are the Legendre polynomials, l is the angular momentum quantum number, ϑ is the polar angle in the spherical coordinate, E is the kinetic energy of the fusion system in the CM frame, and V_L is the interaction potential between the laser field and the nucleus. Note that due to the cylindrical symmetry of the Hamiltonian inside Eq. (1), the wave function $\Psi(t,\boldsymbol{r})$ is independent of the azimuth angle ϕ. $A_{n,l}$ is an unknown scattering coefficient and will be determined in the following subsection. In the intense laser field, as shown in Fig. 1, the charged particle has a series of possible energies $E_n = E + U_p + n\hbar\omega$ for all integers n, where n is the number of photons absorbed or emitted and $U_p = q_{\rm eff}^2 A_0^2/(4\mu)$ is the ponderomotive energy of the particle in the laser fields, respectively. Accordingly, the particle wave number $k_n = \sqrt{2\mu E_n/\hbar^2}$ and dimensionless Coulomb parameter $\eta_n = 1/(k_n a_c)$ in the laser fields, respectively, where $a_c = 4\pi\epsilon_0\hbar^2/(\mu Z_{\rm p}Z_{\rm t}e^2)$ is the Coulomb unit

length. $H_l = F_l - iG_l$, where G_l is an irregular Coulomb wave function [53].

In view of temporal integrals in the exponent inside Eq. (3), by inserting vector potential $\boldsymbol{A}(t)$ into Eq. (3) and exploiting the Jocabi-Anger identity [53], one can obtain

$$\begin{aligned} e^{-\frac{i}{\hbar}\int_{-\infty}^{t} V_L d\tau} &= e^{-\frac{i}{\hbar}\int_{-\infty}^{t}(-\frac{q_{\rm eff}}{\mu}\boldsymbol{A}(t)\cdot\boldsymbol{p}+\frac{q_{\rm eff}^2 A^2}{2\mu})d\tau} \\ &= e^{i(\zeta\sin\omega t-\frac{z}{2}\sin 2\omega t - U_p t)} \\ &= \sum_{-\infty}^{+\infty}\tilde{J}_n\left(\zeta,-\frac{z}{2}\right)e^{-\frac{i}{\hbar}(U_p+n\hbar\omega)t}, \end{aligned} \tag{4}$$

where $\zeta = q_{\rm eff}A_0 p\cos\theta/(\hbar\omega)$, $z = q_{\rm eff}A_0/(4\mu\hbar\omega)$, and $\tilde{J}_n$ is the generalized Bessel function [53]. θ is the angle between the particle momentum $\boldsymbol{P}$ and laser polarization axis (the z axis). Putting Eq. (4) into Eq. (3), $\Psi(t,\boldsymbol{r})$ can be further written as

$$\begin{aligned} \Psi(t,\boldsymbol{r}) = &\sum_{n=-\infty}^{+\infty}\sum_{l=0}^{+\infty}(2l+1)i^l\tilde{J}_n\left(\zeta,-\frac{z}{2}\right)\frac{F_l(k_n r,\eta_n)}{k_n r} \\ &\times P_l(\vartheta)e^{-\frac{i}{\hbar}E_n t} \\ &+\sum_{n=-\infty}^{+\infty}\sum_{l=0}^{+\infty}(2l+1)i^l A_{n,l}\frac{H_l(k_n r,\eta_n)}{k_n r} \\ &\times P_l(\vartheta)e^{-\frac{i}{\hbar}E_n t}, \quad r > r_N. \end{aligned} \tag{5}$$

Similarly, the wave function $\Psi(t,\boldsymbol{r})$ that satisfies the boundary conditions inside nuclear potential well can be given by

$$\begin{aligned} \Psi(t,\boldsymbol{r}) = &\sum_{m,E_{\rm in}}\sum_{l=0}^{+\infty}B_l(E_{\rm in})(2l+1)i^l\tilde{J}_m\left(-\zeta,\frac{z}{2}\right)\frac{j_l(k_N r,\eta)}{k_N r} \\ &\times P_l(\vartheta)e^{-\frac{i}{\hbar}E_m t}, \quad r < r_N, \end{aligned} \tag{6}$$

where $B_l(E_{\rm in})$ is a coefficient, $E_{\rm in}$ is the energy in the nuclear potential, j_l is the Riccati-Bessel function [53], and $k_N = \sqrt{2\mu(E_{\rm in}-V_{\rm r}-iV_{\rm i})/\hbar^2}$ is the complex wave number in the nuclear well. $E_m = E_{\rm in} + U_p + m\hbar\omega$ is the excited energy in the nuclear well after absorbing m photons with a pondermotive potential U_p shift.

B. The continuity conditions of wave function at the radius of nuclear well

The coefficients $A_{n,l}$ inside Eq. (5) are so far unknown and would be determined by means of the the continuity conditions of wave function at the radius of the nuclear well. The continuity conditions of the wave function and its first derivative are satisfied simultaneously at $r = r_N$ for all values of ϑ and t, and one can obtain

$$\begin{aligned} &E_{\rm in} + U_p + m\hbar\omega = E + U_p + n\hbar\omega, \\ &\sum_m B_l(E_{\rm in})j_m(k_N r_N)\tilde{J}_n = F_l(k_n r_N)\tilde{J}_n + A_{n,l}H_l(k_n r_N), \\ &\sum_m B_l(E_{\rm in})k_N j_m'(k_N r_N)\tilde{J}_n = k_n[F_l'(k_n r_N)\tilde{J}_n + A_{n,l}H_l'(k_n r_N)]. \end{aligned} \tag{7}$$

One can easily find that $E_{\rm in} = E + (n-m)\hbar\omega$ and $k_{N,m} = \sqrt{2m(E+(n-m)\omega - V_{\rm r} - iV_{\rm i})/\hbar^2}$. We can define the logarithmic derivative

$$C_{n,l} \equiv \frac{\sum_m B_l(E+(n-m)\omega)k_{N,m}j_l'(k_N r_N)\tilde{J}_m}{\sum_m B_l(E+(n-m)\omega)j_l(k_N r_N)\tilde{J}_m}. \tag{8}$$

We assume $B_l(E+(n-m)\hbar\omega) \approx B_l(E+n\hbar\omega)$ and, according to Eq. (7), one can then find

$$\begin{aligned} A_{n,l} &= \frac{[C_{n,l}F_l(k_n r_N,\eta) - k_n F_l'(k_n r_N,\eta_n)]\tilde{J}_n\left(\zeta,-\frac{z}{2}\right)}{k_n H_l'(k_n r_N,\eta_n) - C_{n,l}H_l(k_n r_N,\eta_n)} \\ &\equiv A_{n,l}^0\tilde{J}_n\left(\zeta,-\frac{z}{2}\right). \end{aligned} \tag{9}$$

C. Multiphoton fusion cross sections

For the evaluation of fusion cross sections in a laser field, we start from the asymptotic form of the wave function $\Psi(t,\boldsymbol{r})$ [i.e., Eq. (5)]. Since, for $r\to+\infty$, $F_l(k_n r,\eta_n) \to [e^{i(k_n r - l\pi/2)} - e^{-i(k_n r - l\pi/2)}]/(2i)$ and $H_l(k_n r,\eta_n) \to -ie^{i(k_n r - l\pi/2)}$, the wave function $\Psi(\boldsymbol{r})$ may be written in asymptotic form as

$$\begin{aligned} \Psi(\boldsymbol{r}\to+\infty) = &\sum_{n=-\infty}^{+\infty}\sum_{l=0}^{+\infty}(2l+1)(-1)^{l+1}\left[\tilde{J}_n\frac{e^{-ikr}}{2ikr}\right. \\ &\left.+(2A_{n,l}+\tilde{J}_n)\frac{e^{ik_n r}}{2ik_n r}\right]\times P_l(\vartheta). \end{aligned} \tag{10}$$

The probability current of the particles in a laser field reads

$$\boldsymbol{J}_{\rm c}(t) = \frac{\hbar}{2im}(\Psi^*\nabla\Psi - \Psi\nabla\Psi^*) - \frac{q}{\mu}\boldsymbol{A}(t)\Psi^*\Psi. \tag{11}$$

The time-average current during a period of the laser field can be written as

$$\bar{\boldsymbol{J}}_{\rm c} = \frac{1}{T}\int_0^T \boldsymbol{J}_{\rm c}(t)dt = \frac{\hbar}{2i\mu}(\Psi^*\nabla\Psi - \Psi\nabla\Psi^*). \tag{12}$$

The time-average current of incoming particles, denoted as $\bar{\boldsymbol{J}}_{\rm c}^{\rm inc}$, is computed from the incoming wave function as

$$\bar{\boldsymbol{J}}_{\rm c}^{\rm inc} = \frac{\hbar}{2i\mu}(\Psi_{\rm inc}^*\nabla\Psi_{\rm inc} - \Psi_{\rm inc}\nabla\Psi_{\rm inc}^*) = \frac{\hbar\boldsymbol{k}_n}{\mu}. \tag{13}$$

The radial component of the time-average current in the laser field is essential for fusion cross section and it reads

$$\bar{J}_{\rm c}^r = \bar{\boldsymbol{J}}_{\rm c}\cdot\hat{e}_r = \frac{\hbar}{2i\mu}\left(\Psi^*\frac{\partial}{\partial r}\Psi - \Psi\frac{\partial}{\partial r}\Psi^*\right). \tag{14}$$

Putting Eq. (10) into Eq. (14), we can find

$$\begin{aligned} \bar{J}_{\rm c}^r = &\sum_{n=-\infty}^{+\infty}\bar{J}_{\rm c}^{rn} = \sum_{n=-\infty}^{+\infty}\sum_{l,l_1}\frac{(2l+1)(2l_1+1)}{4k_n\mu r^2}P_l(\vartheta)P_{l_1}(\vartheta) \\ &\times\left\{(2A_{n,l}^*+\tilde{J}_n)(2A_{n,l_1}+\tilde{J}_n) - (-1)^{l+l_1}\tilde{J}_n^2\right\}. \end{aligned} \tag{15}$$

The differential fusion cross sections in each solid angle can be defined as

$$\frac{d\sigma(E,\theta,\vartheta)}{d\Omega} = \sum_{n=-\infty}^{+\infty}\frac{d\sigma_n(E,\theta,\vartheta)}{d\Omega} = \sum_{n=-\infty}^{+\infty}\frac{\bar{J}_{\rm c}^{rn}r^2 d\Omega}{\bar{J}_{\rm c}^{\rm inc}d\Omega}. \tag{16}$$

By the integrating over the solid angle $d\Omega$, we can easily obtain the total fusion cross sections:

$$\begin{aligned}\sigma(E,\theta) &= \sum_{n=-\infty}^{+\infty}\sigma_n(E,\theta) = \sum_{n=-\infty}^{+\infty}\int\frac{d\sigma_n(E,\vartheta,\theta)}{d\Omega}\sin\vartheta\, d\vartheta \\ &= \sum_{n,l=-\infty}^{+\infty}\frac{(2l+1)\pi\left(\tilde{J}_n^2 - |2A_{n,l}+\tilde{J}_n|^2\right)}{k_n^2} \\ &= \sum_{n,l=-\infty}^{+\infty}\frac{(2l+1)\pi\left(1-|2A^0_{n,l}+1|^2\right)}{k_n^2}\tilde{J}_n^2\left(\zeta,-\frac{z}{2}\right) \\ &\equiv \sum_{n,l=-\infty}^{+\infty}\sigma_l(E_n)P_n(\theta). \end{aligned} \tag{17}$$

Equation (17) has a clear physical interpretation, representing the product of the cross section $\sigma_l(E_n)$ associated with the possible energy E_n of a charged particle and the corresponding probability $P_n(\theta) = \tilde{J}_n^2(\zeta, -\frac{z}{2})$ of the particle absorbing or emitting photons in intense laser fields. It is noteworthy that $\sum_n P_n(\theta) = 1$.

III. NUMERICAL RESULTS AND DISCUSSIONS

In the context of the low-energy ($E < 1$ MeV) fusion reaction in the following calculations, our focus is only on computing the S wave ($l = 0$) contribution to the cross section. In a low-frequency intense laser field, the energy of the laser photon (on the order of eV) is significantly less than the both absolute value of the real part $|V_r|$ (on the order of MeV) of the optical potential and the collision energy E (on the order of keV) so that the complex wave number in the nuclear well $k_{N,m} \approx \sqrt{2\mu(E - V_r - iV_i)/\hbar^2}$. This result implies that a low-frequency intense field primarily alters the energy of fusion particles.

A. Multiphoton fusion cross sections of DT fusion

1. Distributions of multiphoton fusion cross sections

We first examine the distributions of multiphoton fusion cross sections σ_n concerning the number of absorbed ($n > 0$) or emitted ($n < 0$) laser photons for DT fusion. Examples of σ_n are presented in Fig. 2 for wavelengths of 800 and 100 nm, employing a consistent laser intensity of 10^{20} W/cm^2 and the relative kinetic energy of $E = 5$ keV. Two angles θ are indicated for each wavelength. The number of laser photons involved in the fusion reaction is highly dependent on both the laser wavelength and the angle between the incident direction of the particle and the laser polarization axis. As seen in Figs. 2(a) and 2(c), as the laser wavelength shortens, the number of photons involved decreases from over 2000 photons (800 nm) to only 120 photons (100 nm). This is partly due to the fact that shorter wavelength results in fewer photons per unit area for the fixed laser intensity. On the other hand, Figs. 2(a) and 2(b) demonstrate that as the angle changes from inclination angle $\theta = 0$ (i.e., the incident direction of the particle is parallel to the laser polarization direction) to $\theta = \pi/2$ (i.e., the direction perpendicular to the polarization direction), the number of laser photons involved becomes smaller, while the peak values of the multiphoton cross sections increase. Notably, understanding the presence of laser photons at $\theta = \pi/2$ proves challenging within the classical framework.

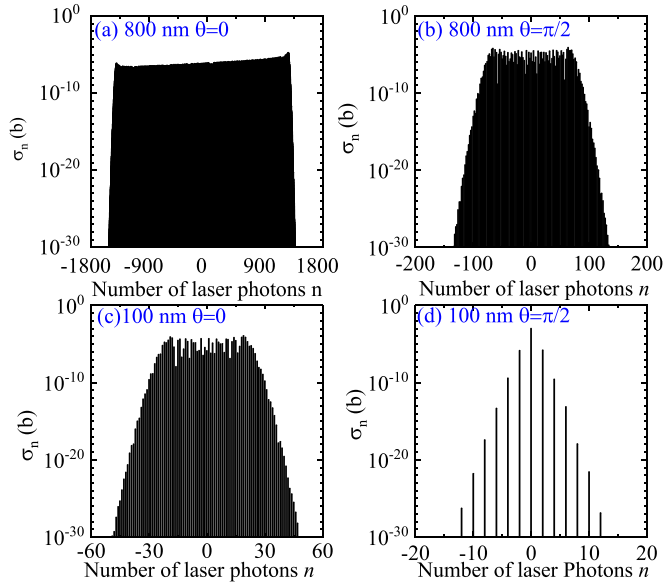

FIG. 2. (a)–(d) Distributions of the multiphoton cross sections σ_n for laser-assisted DT fusion as a function of the number of absorbed ($n > 0$) or emitted ($n < 0$) laser photons. The laser intensity is 10^{20} W/cm^2 and the relative kinetic energy of DT nuclei $E = 5$ keV for the two laser wavelengths 800 nm (top row) and 100 nm (bottom row). For each wavelength, two θ are shown as labeled in the figure.

Moreover, Figs. 2(a)–2(c) reveal a distinct nonperturbative plateau structure: the multiphoton cross sections decrease rapidly when the number of absorbed or emitted laser photons exceeds a certain threshold. In conclusion, we highlight that total cross sections $\sigma = \sum_n \sigma_n$ in Figs. 2(a)–2(d) are approximately 6.5×10^{-4} b, 2.7×10^{-4} b, 2.3×10^{-4} b, and 2.3×10^{-4} b, respectively. Surprisingly, the results for the laser wavelength 100 nm [Figs. 2(c)–2(d)] indicate that the presence of the laser field contributes the the photoparticle energies over a broad range, but it hardly affects the total cross sections compared with the field-free case (2.3×10^{-4} b). It is worth noting that a similar phenomenon also occurs in the distributions of the multiphoton cross sections for laser-assisted proton emission in Ref. [54].

2. Angle-averaged effective fusion cross section

In the thermal environment of nuclear fusion, the angle between the incident particle wave number $\boldsymbol{k}$ and laser polarization axis is random. To provide a more quantitative measure, the angle-averaged effective fusion cross section in the laser fields can be expressed as [17,20]

$$\sigma_L(E) = \frac{1}{2}\int_0^\pi \sigma(E,\theta)\sin\theta\, d\theta. \tag{18}$$

We display angle-averaged effective cross section σ_L of DT fusion in Fig. 3 under different laser intensities and

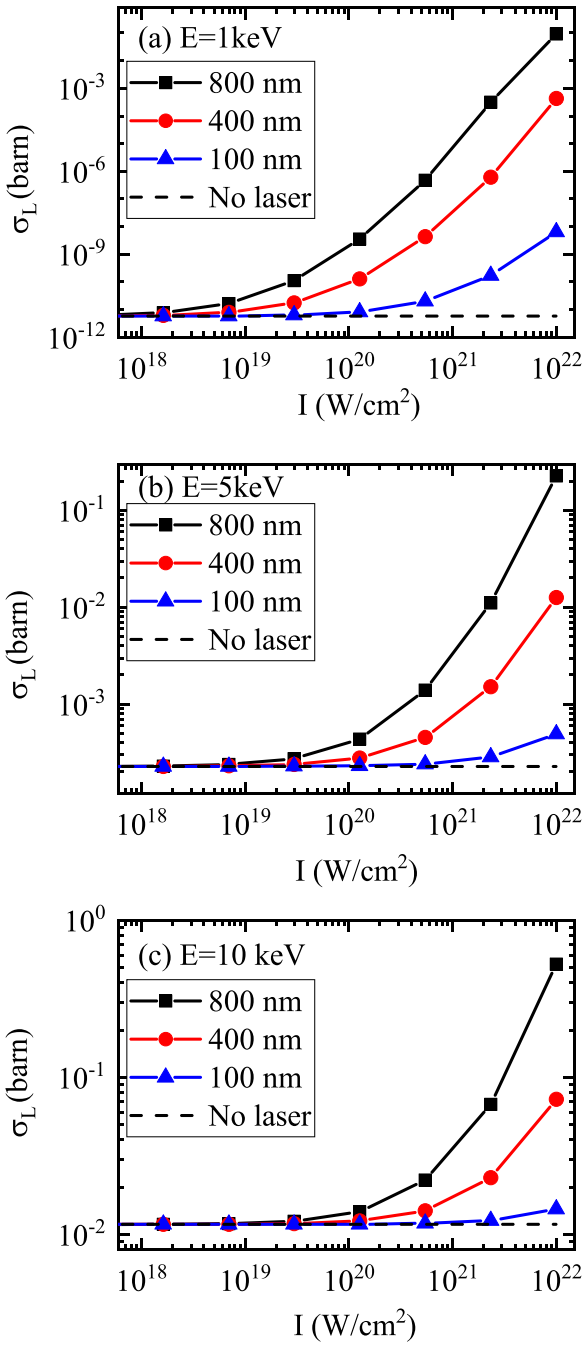

FIG. 3. Angle-averaged effective DT fusion cross section σ_L under different laser intensities and wavelengths for (a) $E = 1$ keV, (b) 5 keV, and (c) 10 keV. The horizontal dashed line in each figure marks the corresponding laser-free cross section.

wavelengths. These laser parameters are anticipated in intense laser facilities worldwide [9,10,48]. Three specific kinetic energies (a) $E = 1$ keV, (b) 5 keV, and (c) 10 keV in Fig. 3 are relevant to controlled fusion research [42]. The horizontal dashed line in each figure marks the corresponding laser-free cross section.

One can observe in Fig. 3 that, for all three energies, the σ_L are substantially enhanced compared to the corresponding laser-free case, with intensities on the order of 10^{22} W/cm^2.

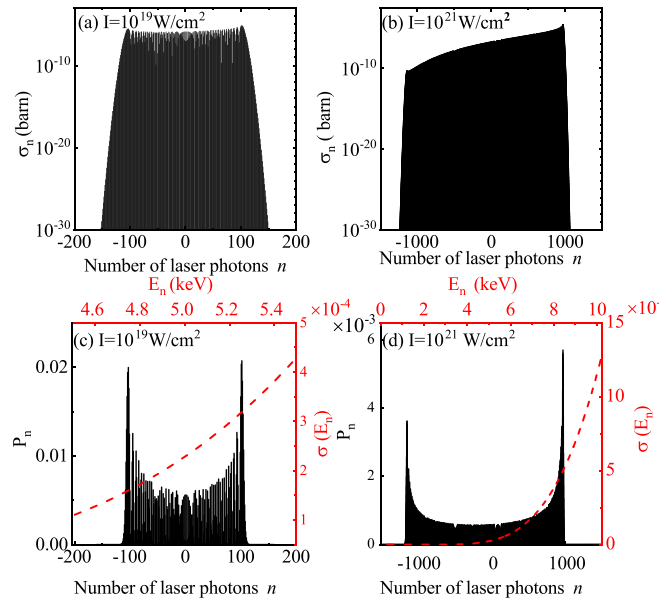

FIG. 4. Distributions of the multiphoton cross sections σ_n as a function of the number of absorbed ($n > 0$) or emitted ($n < 0$) laser photons for two intensities (a) $I = 10^{19}$ W/cm^2 and (b) 10^{21} W/cm^2. (c)–(d) Corresponding distributions of the probability P_n (black solid lines) and cross section $\sigma(E_n)$ (red dot lines). The laser wavelength, the relative kinetic energy of DT nuclei and the incident angle are 400 nm, 5 keV, and 0, respectively.

Moreover, Fig. 3 illustrates that with longer laser wavelength and low relative kinetic energy E, the laser field can more efficiently transfer energy to the DT fusion system, resulting in higher σ_L. For instance, at a laser wavelength of 800 nm and a relative kinetic energy of 1 keV, the σ_L increases by approximately ten orders of magnitude. However, for a laser wavelength of 100 nm and a relative kinetic energy of 10 keV, the σ_L only exhibits a onefold increase.

To gain a deeper understanding of the enhanced fusion cross sections with increasing laser intensity, we focus on two scenarios: (a) $I = 10^{19}$ W/cm^2 and (b) $I = 10^{21}$ W/cm^2 in Fig. 4 for detailed discussions. Other fixed parameters, including the the laser wavelength (400 nm), the relative kinetic energy of DT nuclei (5 keV), and the incident angle (0), remain constant. We present the distributions of multiphoton cross sections as a function of the number of laser photons in Figs. 4(a) and 4(b). It is evident from these figures that as the laser intensity increases, the number of laser photons involved in the DT fusion process significantly increase. Specifically, at a laser intensity of $I = 10^{19}$ W/cm^2, three hundred laser photons are involved in fusion process, while, at $I = 10^{21}$ W/cm^2, more than two thousand laser photons are involved. Additionally, the multiphoton distribution exhibits a pronounced asymmetry with increasing laser intensity.

Simultaneously, we present the corresponding distributions of the probability P_n (black solid lines) and cross section $\sigma(E_n)$ (red dot lines) in Figs. 4(c) and 4(d) for possible energy E_n of the particle under an intense laser field. It is crucial to note that multiphoton cross section σ_n is calculated

as the product of probability P_n and cross section $\sigma(E_n)$ associated with the possible energy E_n, as defined by Eq. (17).

In Fig. 4(c), it is evident that as the number of absorbed or emitted photons increases, the probability P_n also increases. The symmetrical structure of P_n with respect to $n = 0$ in Fig. 4(c) indicates that the probability of absorbed photons in the fusion process is equivalent to the probability of emitting photons. Additionally, Fig. 4(c) reveals that, at a laser intensity of $I = 10^{19}$ W/cm^2, the possible energy of fusion particle involved in the fusion process is $4.7 < E_n < 5.3$ keV. Correspondingly, the cross section $\sigma(E_n)$ exhibits a monotonic and gradual increase E_n, resulting in $\sum_n \sigma_n(E,\theta) \approx \sigma(E)\sum_n P_n(\theta) = \sigma(E)$. Consequently, in Fig. 3 (c), when the laser wavelength and intensity are 400 nm and 10^{19} W/cm^2, the enhancement of fusion cross section in the laser field is almost negligible.

However, with an increase in laser intensity ($I = 10^{21}$ W/cm^2), the probability distribution P_n in Fig. 4(d) displays a pronounced left-right asymmetry concerning $n = 0$: the probability of absorbing photons exceeds that of emitted photons for a large number of photons. Additionally, compared to the scenario in Fig. 4(c), the possible energy E_n of the particles involved in the fusion process has a large range, from 1 to 9 keV. The corresponding cross section $\sigma(E_n)$ also exhibits a rapid and monotonic increase with E_n. The increased number of involved photons and higher probability of absorbing laser photons contribute to an enhanced fusion cross section under laser fields with a wavelength of 400 nm and an intensity of $I = 10^{21}$ W/cm^2 in Fig. 3(b). In summary, the rise in laser intensity leads to a monotonic increase in both the number of laser photons involved in the fusion process and the corresponding absorption probability, resulting in a monotonically enhanced cross section in Fig. 3.

B. Multiphoton cross sections of p ^{11}B fusion

In this section, our focus is on the p ^{11}B fusion reaction. We have calibrated three optical parameters V_r, V_i, and r_n for p ^{11}B fusion at low energy using precise Coulomb wave functions [47]. Subsequently, we investigate the multiphoton effect of p ^{11}B fusion. Distributions of multiphoton cross sections for the p ^{11}B fusion resemble those of DT fusion and they are not presented here. Angle-averaged effective cross sections σ_L of p ^{11}B fusion are displayed in Fig. 5 under various laser intensities and wavelengths for the relative kinetic energies (a) $E = 20$ keV, (b) 50 keV, and (c) 100 keV, respectively. The horizontal dashed line in each figure indicates the corresponding laser-free cross section.

The data presented in Fig. 5 indicate that, for all three kinetic energies, σ_L are enhanced compared to the corresponding laser-free case under high laser intensities. Similar to DT fusion, when considering a longer laser wavelength and low kinetic energy E, the σ_L for p ^{11}B fusion exhibits substantial increases in comparison to the laser-free case. Specifically, at a constant laser intensity $I = 10^{23}$ W/cm^2, the σ_L exhibits a nearly four-order-of-magnitude increase for a laser wavelength of 800 nm and kinetic energy of 20 keV. In contrast, for a laser wavelength of 100 nm and kinetic energy of 100 keV, the increase is only a 0.2-fold, as depicted in Fig. 5.

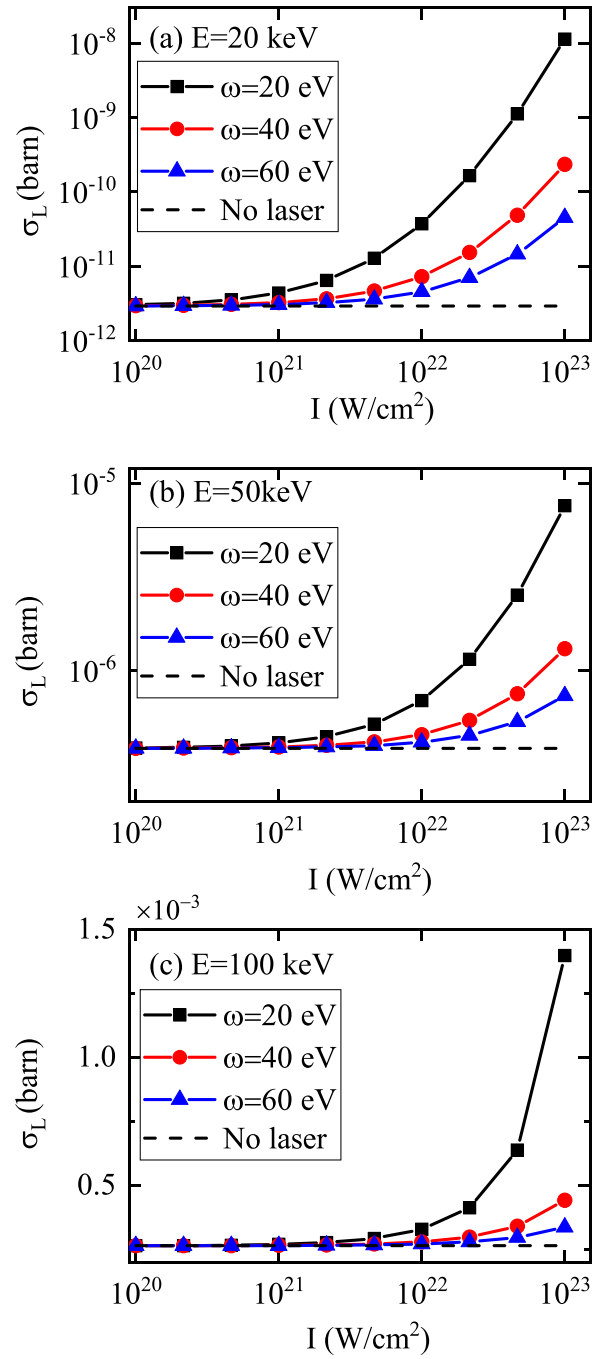

FIG. 5. Angle-averaged effective p ^{11}B fusion cross section σ_L under different laser intensities and wavelengths for (a) $E = 20$ keV, (b) 50 keV, and (c) 100 keV. The horizontal dashed line in each figure marks the corresponding laser-free cross section.

Furthermore, compared to DT fusion results, higher laser intensities are necessary to influence the cross section of p ^{11}B fusion reaction due to the elevated Coulomb repulsion barriers.

C. Some discussions

Our findings demonstrate the significant enhancements of the fusion cross sections for both DT and p ^{11}B fusion re-

actions under intense laser fields. Some discussions on the origin and mechanism of this enhancement are crucial and intriguing. As is well known, in the Gamow picture [41,42], the nuclear fusion can be separated by phenomenon into three steps, i.e., the Coulomb collision before tunneling, tunneling through Coulomb potential, and the fusion process dominated by nuclear force. Extending the Gamow picture to the situation where intense laser fields are present, ones find a similar substantial enhancement for DT fusion [20,28,30,31]. The underlying mechanism is due to the particle acceleration in the first period before tunneling. However, these approaches do not consider the nuclear potential [20,28,30,31] or the Coulomb repulsion potential [20]. Our present work develops a full quantum description to calculate the fusion cross sections, considering both the complex spherical square-well nuclear potential and the Coulomb potential. Utilizing the Coulomb-Volkov solutions, we have derived the multiphoton cross sections of nuclear fusion in a self-consistent way. Our present calculations focus on the laser wavelengths in the optical or near-optical regime. In this case, the wave functions inside the nuclear well are hardly excited by the laser fields because the photon energy ($\sim$ the order of eV) of laser fields is too small compared to the nuclear energy level ($\sim$ the order of MeV). The enhancement mechanism of the fusion cross sections is mainly caused by the laser-dressed Coulomb waves [i.e., expressed by Eq. (5)] outside the nuclear well via multiphoton processes. In the quantum-classical correspondence, the multiphoton enhancement mechanism in the optical or near-optical regime might resemble the laser-assisted particle acceleration effect as depicted in the semiclassical picture [28]. However, for higher frequency lasers such as hard x rays or γ rays, the multiphoton effects might alter the waves inside the nuclear well, which merits further investigations.

IV. CONCLUSIONS AND OUTLOOKS

In conclusion, we have examined the physics of multiphoton fusion reactions involving light nuclei such as DT and p ^{11}B. This investigation incorporates a combination of the Coulomb-Volkov solutions and the complex spherical square-well nuclear potential. Our theoretical findings reveal that, particularly with longer laser wavelengths and lower incident particle kinetic energies, several thousand photons can participate in the fusion reactions, resulting in a significant enhancement of fusion cross section. Additionally, we observe distinct nonperturbative plateau structures in the distributions of multiphoton cross sections. These outcomes suggest that intense low-frequency lasers could prove instrumental in advancing controlled fusion research, potentially relaxing the temperature requirements outlined in the well-known Lawson criterion [55]

In this study, we exclusively examine the low-frequency regime of laser fields. The γ-ray-assisted multiphoton fusion processes involving nuclear excitation merit further exploration. Furthermore, it is essential to acknowledge that the complex spherical square well represents the most basic optical model for describing the nuclear potential during fusion. Future investigations should contemplate the utilization of a more realistic optical potential featuring a rigid core and nuclear spin, such as the Woods-Saxon forms [56], particularly in the context of multiphoton fusion processes.

ACKNOWLEDGMENT

This work was supported by funding from NSAF Grant No. U2330401 and from the National Natural Science Foundation of China Grants No. 12375235 and No. 12174034.

[1] C. J. Joachain, N. J. Kylstra, and R. M. Potvliege, *Atoms in Intense Laser Fields* (Cambridge University Press, Cambridge, 2012).
[2] J. Liu, *Classical Trajectory Perspective of Atomic Ionization in Strong Laser Fields* (Springer, Berlin, 2014).
[3] E. K. Damon and R. G. Tomlinson, Appl. Opt. **2**, 546 (1963).
[4] G. Mainfray and G. Manus, Rep. Prog. Phys. **54**, 1333 (1991).
[5] G. G. Paulus, W. Nicklich, H. Xu, P. Lambropoulos, and H. Walther, Phys. Rev. Lett. **72**, 2851 (1994).
[6] B. Walker, B. Sheehy, L. F. DiMauro, P. Agostini, K. J. Schafer, and K. C. Kulander, Phys. Rev. Lett. **73**, 1227 (1994).
[7] A. McPherson, G. Gibson, H. Jara *et al.*, J. Opt. Soc. Am. B **4**, 595 (1987).
[8] M. Ferray, A. L'Huillier, X. F. Li *et al.*, J. Phys. B: At. Mol. Opt. Phys. **21**, L31 (1988).
[9] J. W. Yoon, Y. G. Kim, I. W. Choi, J. H. Sung, H. W. Lee, S. K. Lee, and C. H. Nam, Optica **8**, 630 (2021).
[10] http://www.eli-np.ro
[11] C. B. Fu, G. Q. Zhang, and Y. G. Ma, Matter Radiat. Extremes **7**, 024201 (2022).
[12] W. Wang, J. Zhou, B. Q. Liu, and X. Wang, Phys. Rev. Lett. **127**, 052501 (2021).
[13] J. Qi, H. Zhang, and X. Wang, Phys. Rev. Lett. **130**, 112501 (2023).
[14] D. S. Delion and S. A. Ghinescu, Phys. Rev. Lett. **119**, 202501 (2017).
[15] D. Bai, D. Deng, and Z. Ren, Nucl. Phys. A **976**, 23 (2018).
[16] D. Bai and Z. Z. Ren, Commun. Theor. Phys. **70**, 559 (2018).
[17] S. A. Ghinescu and D. S. Delion, Phys. Rev. C **101**, 044304 (2020).
[18] F. Queisser and R. Schützhold, Phys. Rev. C **100**, 041601(R) (2019).
[19] W. J. Lv, H. Duan, and J. Liu, Phys. Rev. C **100**, 064610 (2019).
[20] X. Wang, Phys. Rev. C **102**, 011601(R) (2020).
[21] S. W. Liu, H. Duan, D. F. Ye, and J. Liu, Phys. Rev. C **104**, 044614 (2021).
[22] C. Kohlfürst, F. Queisser, and R. Schützhold, Phys. Rev. Res. **3**, 033153 (2021).
[23] W. J. Lv, B. Wu, H. Duan, S. W. Liu, and J. Liu, Eur. Phys. J. A **58**, 54 (2022).
[24] J. T. Qi, Nucl. Phys. A **1020**, 122394 (2022).
[25] B. Wu, H. Duan, and J. Liu, Phys. Rev. C **105**, 064615 (2022).
[26] J. J. Bekx, M. L. Lindsey, S. H. Glenzer, and K. G. Schlesinger, Phys. Rev. C **105**, 054001 (2022).

[27] J. J. Bekx, M. L. Lindsey, and K. G. Schlesinger, Phys. Rev. C **106**, 034003 (2022).
[28] S. W. Liu, D. F. Ye, and J. Liu, Phys. Rev. C **106**, 064611 (2022).
[29] D. Ryndyk, C. Kohlfürst, F. Queisser, and R. Schützhold, Phys. Rev. Res. **6**, 023056 (2024).
[30] M. L. Lindsey, Ph.D. thesis, Stanford University, 2023.
[31] M. L. Lindsey, J. J. Bekx, K. G. Schlesinger, and S. H. Glenzer, Phys. Rev. C **109**, 044605 (2024).
[32] D. E. Kharzeev and J. Levitt, arXiv:2311.03492.
[33] I. V. Kopytin and A. S. Kornev, Phys. At. Nuclei **77**, 53 (2014).
[34] K. I. Vasilievich, Am. J. Phys. Appl. **7**, 89 (2019).
[35] J. T. Qi, T. Li, R. H. Xu, L. B. Fu, and X. Wang, Phys. Rev. C **99**, 044610 (2019).
[36] A. Pálffy and S. V. Popruzhenko, Phys. Rev. Lett. **124**, 212505 (2020).
[37] J. T. Qi, L. B. Fu, and X. Wang, Phys. Rev. C **102**, 064629 (2020).
[38] Z. U. Rehman, N. Shabbir, S. Shafiq, and A. Shahbaz, Eur. Phys. J. A **58**, 60 (2022).
[39] J. H. Cheng, W. Y. Zhang, Q. Xiao, J. G. Deng, and T. P. Yu, Phys. Lett. B **848**, 138322 (2024).
[40] J. H. Cheng, W. Y. Zhang, Q. Xiao, J. G. Deng, and T. P. Yu, arXiv:2307.02095v1.
[41] G. Gamow, Z. Phys. **51**, 204 (1928).
[42] S. Atzeni and J. Meyer-ter-Vehn, *The Physics of Inertial Fusion Beam Plasma Interaction, Hydrodynamics, Hot Dense Matter* (Clarendon, Oxford, 2004).
[43] W. H. Dickhoff and R. J. Charity, Prog. Part. Nucl. Phys. **105**, 252 (2019).
[44] X. Z. Li, J. Tian, M. Y. Mei, and C. X. Li, Phys. Rev. C **61**, 024610 (2000).
[45] X. Z. Li, Q. M. Wei, and B. Liu, Nucl. Fusion **48**, 125003 (2008).
[46] V. Singh, D. Atta, Md. A. Khan, and D. N. Basu, Nucl. Phys. A **986**, 98 (2019).
[47] B. Wu, H. Duan, and J. Liu, Nucl. Phys. A **1017**, 122340 (2022).
[48] Z. Zhang, F. Wu, J. Hu *et al.*, High Power laser Sci. Eng. **8**, e4 (2020).
[49] F. Ehlotzky, A. Jaroń, and J. Z. Kamiński, Phys. Rep. **297**, 63 (1998).
[50] W. J. Lv, H. Duan, and J. Liu, Nucl. Phys. A **1025**, 122490 (2022).
[51] A. Tentori and F. Belloni, Nucl. Fusion **63**, 086001 (2023).
[52] V. Istokskaia, M. Tosca, L. Giuffrida *et al.*, Commun. Phys. **6**, 27 (2023).
[53] M. Abramowitz and I. A. Stegun, *Handbook of Mathematical Functions with Formulas, Graphs, and Mathematical Tables* (Dover, New York, 1972).
[54] A. Dadi and C. Muller, Phys. Rev. C **85**, 064604 (2012).
[55] J. D. Lawson, Proc. Phys. Soc. B **70**, 6 (1957).
[56] J. O. Newton, R. D. Butt, M. Dasgupta, D. J. Hinde, I. I. Gontchar, C. R. Morton, and K. Hagino, Phys. Rev. C **70**, 024605 (2004).